Thin magnetosheath as a consequence of the magnetopause deformation: THEMIS observations

K. Jelínek,[1] Z. Němeček,[1] J. Šafránková,[1] J.-H. Shue,[2] A. V. Suvorova,[2,3] and D. G. Sibeck[4]

Received 8 February 2010; revised 14 May 2010; accepted 24 May 2010; published 2 October 2010.

[1] This paper presents a simultaneous observation of the bow shock and magnetopause by THEMIS probes that allows determination of the actual magnetosheath thickness at the subsolar point. Moreover, Geotail located at the dusk dayside magnetosheath registered a brief excursion to the magnetosphere in this time. The spacecraft configuration reveals a significant deformation of the magnetopause surface that locally decreases its curvature radius. The highly curved magnetopause results in the decrease of the magnetosheath thickness to about half of its standard value in a particular observation point. The observed phenomenon is attributed to a rotation of the interplanetary magnetic field (IMF). Although it is generally expected that the bow shock and magnetopause move in accord, being driven mainly by the solar wind dynamic pressure, we suggest that the local and transient thinning of the magnetosheath can result from different responses of its boundaries to a sudden change of the pressure and/or IMF orientation.

Citation: Jelínek, K., Z. Němeček, J. Šafránková, J.-H. Shue, A. V. Suvorova, and D. G. Sibeck (2010), Thin magnetosheath as a consequence of the magnetopause deformation: THEMIS observations, *J. Geophys. Res.*, *115*, A10203, doi:10.1029/2010JA015345.

1. Introduction

[2] The bow shock and magnetopause are formed by interaction of the solar wind and interplanetary magnetic field (IMF) with the Earth's magnetic field, and the magnetosheath is a region separating these boundaries. Using aerodynamics, *Seiff and Whiting* [1962] empirically showed that the standoff distance of the bow shock normalized by the radius of the obstacle (magnetopause) is nearly linearly proportional to the inverse density ratio across the bow shock. The relationship is as follows:

$$\frac{\Delta_{msh}}{a_{mp}} = 1.1\,\frac{\rho_{sw}}{\rho_{msh}} \tag{1}$$

where ρ is the density, Δ_{msh} is the standoff distance of the bow shock from the obstacle (equivalently, the magnetosheath thickness), a_{mp} is the distance from the center to the nose of the obstacle, and the subscripts indicate the upstream (*sw*) and the downstream (*msh*) states. The bow shock distance from the Earth, a_s is estimated as follows:

$$a_s = a_{mp} + \Delta_{msh}. \tag{2}$$

[3] *Spreiter et al.* [1966] applied this knowledge to gas-dynamic flow around a magnetosphere and showed that the density ratio is related to the compressibility of the medium and the asymptotic free-stream Mach number, M, thus the relationship between these quantities is as follows:

$$\frac{\Delta_{msh}}{a_{mp}} = 1.1\,\frac{(\gamma-1)M^2+2}{(\gamma+1)M^2} \tag{3}$$

where γ is the polytropic index. This expression was later included into the bow shock model by *Formisano et al.* [1973]. The coefficient of 1.1 is supposed to be valid for explanation of the bow shock position in front of a blunt obstacle [*Seiff and Whiting*, 1962]. However, *Spreiter et al.* [1966] did not change the shape of the obstacle to test whether this value is valid for other blunt obstacles.

[4] *Farris and Russell* [1994] discussed the magnetosheath thickness and argued that it should be a function of the curvature radius, R_C of the obstacle. The authors modified the relation (3) to take into account this radius. Moreover, they pointed out that this relation provides a finite magnetosheath thickness for $M = 1$ and suggested a new expression that becomes the following:

$$a_s = R_C\left(\frac{a_{mp}}{R_C} + 0.8\,\frac{(\gamma-1)M^2+2}{(\gamma+1)(M^2-1)}\right). \tag{4}$$

[1]Faculty of Mathematics and Physics, Charles University, Prague, Czech Republic.
[2]Institute of Space Science, National Central University, Jhongli, Taiwan.
[3]Skobeltsyn Institute of Nuclear Physics, Moscow State University, Moscow, Russia.
[4]NASA Goddard Flight Center, Greenbelt, Maryland, USA.

Copyright 2010 by the American Geophysical Union.
0148-0227/10/2010JA015345

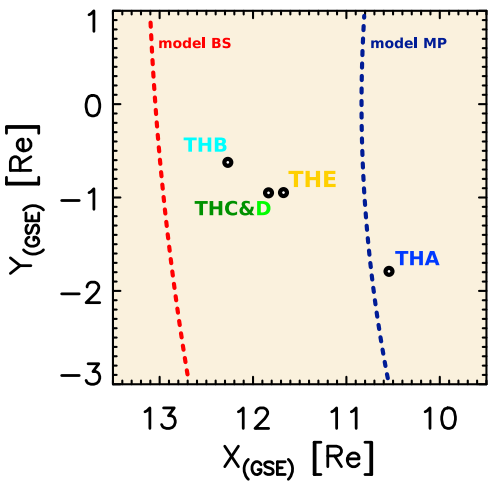

Figure 1. Locations of the THEMIS probes in the *X*-*Y* plane (in the GSE system) at 20 UT. The *Z* coordinates were between −3.3 R_E (THB) and −2.8 R_E (THA). Model magnetopause [*Shue et al.*, 1998] and bow shock [*Jeřáb et al.*, 2005] are showed by the blue and red dotted curves, respectively.

The correction puts the bow shock to infinity for $M = 1$ as one would intuitively expect. It would be noted that the discussed equations were derived using a gas dynamic approach where the Mach number has a clear meaning. A variety of wave modes propagating through the magnetized plasma with different speeds leads to definitions of their own Mach numbers; e.g., sonic, Alfvén, or magnetosonic Mach numbers.

[5] On the other hand, *Němeček and Šafránková* [1991] replaced the factor of 1.1 in (3) with a term that includes the IMF strength and used explicitly the Alfvénic Mach number. This approach was later precised by *Jeřáb et al.* [2005]. Further, *Cairns and Grabbe* [1994] developed an MHD theory for the bow shock standoff distance, a_s and thickness Δ_{msh} of the magnetosheath predicting that the ratio of Δ_{msh}/a_{mp} should depend strongly on θ, M_A and M_S, the angle between the magnetic field and flow, Alfvénic and sonic Mach numbers, respectively, for $M_A \leq 6$.

[6] We can conclude that the magnetosheath thickness is given by the difference between the locations of the bow shock and magnetopause, thus their motion in response to varying upstream conditions changes its thickness. However, the statistical models of these boundaries have different sets of driving parameters; only the solar wind dynamic pressure is common. For example, a dependence of the magnetopause location on the IMF B_Z sign is well established in magnetopause models [e.g., *Fairfield*, 1971; *Sibeck et al.*, 1991; *Roelof and Sibeck*, 1993; *Petrinec and Russell*, 1996; *Shue et al.*, 1997; *Boardsen et al.*, 2000] but the analysis in both *Jeřáb et al.* [2005] and *Merka et al.* [2005] shows that the bow shock does not respond to IMF B_Z changes.

[7] Furthermore, an influence of other parameters on locations of both boundaries was examined in different papers; for example, a rotation of the direction of the magnetic field across the magnetosheath [*Pudovkin et al.*, 1982], both IMF polar and azimuthal angles, and the angle between the IMF and the bow shock normal [*Laakso et al.*, 1998; *Šafránková et al.*, 2003], IMF B_Y component [*Sibeck et al.*, 2000], or Alfvénic fluctuations dominating the solar wind [*Tsubouchi et al.*, 2000]. Moreover, larger displacements of boundaries as a result of their interaction with different solar wind discontinuities (e.g., HFAs, strong interplanetary shocks, pressure pulses) were widely discussed by many authors [e.g., *Sibeck et al.*, 1999; *Farrugia et al.*, 2008; *Zhang et al.*, 2009; *Jacobsen et al.*, 2009].

[8] We went through THEMIS observations of the subsolar bow shock and magnetopause at the 2007–2009 years and found more than 10 cases when the whole magnetosheath was swept along the probes in 2–5 minutes. Since the typical values of speeds of the magnetopause [*Haaland et al.*, 2004] and bow shock [e.g., *Lepidi et al.*, 1996; *Šafránková et al.*, 2003] displacements are about 30–60 km/s, these observations suggest that the magnetosheath can be very thin (or the speeds of boundary displacements are very large) under some circumstances.

[9] The present paper discusses one case when the bow shock and magnetopause were observed simultaneously by two THEMIS probes and the magnetosheath thickness can be unambiguously estimated. We show that the thin magnetosheath is a consequence of a transient deformation of the magnetopause surface resulting in a locally decreased curvature radius. The magnetopause deformation is probably connected with the change of the IMF orientation.

2. Observations

[10] As shown in Figure 1, all THEMIS probes scanned the subsolar bow shock and magnetopause on the late afternoon of 16 July 2007. The locations of probes in GSE coordinates, times, and normals of the boundary crossings are listed in Table 1. The magnetopause normals are determined from magnetic field measurements [*Auster et al.*, 2008] by a minimum variance method, and the bow shock normals are calculated using magnetic coplanarity theorem. Table 1 also contains the parameters of crossings observed nearly simultaneously by Geotail at the dayside dusk magnetosheath.

[11] IMF and solar wind parameters propagated from the ACE (+225; −2; +23 R_E in GSE) and Wind (+253; −67; +17 R_E in GSE) locations toward THEMIS B (THB) together with Geotail observations in the magnetosheath are shown in Figure 2. We applied a standard two-step propagation method. In the first step, an auxiliary time lag between both spacecraft is computed under an assumption that the solar wind speed is 450 km/s. The real velocity measured by an upstream monitor at the time given by this auxiliary lag is then used for a determination of the final lag. Such procedure was applied to each point of the THB measurements for both solar wind monitors.

[12] The upstream density (first image) and velocity (second and third images) were very similar and stable on both monitors throughout the depicted interval. The same is true for the magnetic field magnitudes (fourth and fifth images). Consequently, typical driving parameters: the upstream dynamic pressure ($p_{SW} \sim 1.3$ nPa) and Mach number ($M_A \sim 11$) were about constant, and they cannot be responsible for observed displacements of boundaries. On the other hand, the IMF direction changed several times

Table 1. Survey of Magnetopause and Bow Shock Crossings Observed by THEMIS and Geotail[a]

Spacecraft	Time (UT)	Boundary	GSE Position [R_E]			n_{MP}/n_{BS}			Event
TH-B	2020:43.7	MP	12.11	−0.74	−3.33	−0.997	0.028	0.066	1
	2024:43.7	MP	12.16	−0.71	−3.34	−0.884	0.305	0.355	2
	*2032:43.7	MP	12.24	−0.65	−3.37	−0.794	0.321	0.516	3
	†2037:23.1	BS	12.28	−0.61	−3.38	−0.961	0.167	0.219	9
	2039:10.0	BS	12.30	−0.60	−3.39	−0.701	0.263	−0.663	11
TH-D	*2033:30.6	MP	11.83	−0.99	−3.23	−0.823	0.306	0.479	4
TH-C	*2033:32.5	MP	11.82	−0.95	−3.24	−0.859	0.186	0.477	5
TH-E	*2034:34.3	MP	11.68	−0.95	−3.22	−0.830	0.176	0.529	6
TH-A	*2036:13.7	MP	10.54	−1.80	−2.82	−0.899	0.107	0.424	7
	2036:30.6	MP	10.55	−1.80	−2.82	−0.422	−0.472	0.774	8
	†2037:41.8	MP	10.56	−1.79	−2.83	−0.338	−0.851	−0.402	10
	2042:04.3	MP	10.63	−1.76	−2.85	−0.959	0.271	0.088	14
Geotail	2039:45.0	MP	5.48	15.64	1.09	−0.635	−0.762	0.128	12
	2042:00.0	MP	5.45	15.67	1.08	−0.054	−0.734	−0.677	13

[a]The columns indicate the spacecraft name, times of boundary crossings of a particular spacecraft, the boundary crossed, coordinates of the crossing in GSE, estimated normals, and event numbers that are used in the figures. The asterisks denote the times used for calculation of a mean magnetopause normal and speed by the triangulation method, and the daggers stand for the bow shock and magnetopause crossings used for a determination of the instantaneous magnetosheath thickness.

and differs at ACE and Wind locations as it can be seen from IMF components and cone angles (sixth image). The cone angle was computed as the angle between the X_{GSE} axis and the IMF direction. Since the IMF orientation is principal for an interpretation of results, we add to the IMF images the THB magnetic field (as diamonds) for an interval around ≈2038 UT when it was located in the solar wind just upstream of the quasi-perpendicular bow shock. One can note that B_Y (green points) is the only nonzero component (≈4 nT) in THB observations.

[13] The last three images show the Geotail magnetic field, electron spectra, and five channels of the EPIC energetic ions. The energy of electrons, together with a moderate and fluctuating magnetic field, indicate that Geotail was in the magnetosheath for the whole interval except a short excursion into the magnetosphere at ≈2040 UT (see Table 1 for timing). A strongly spin-modulated flux of energetic particles suggests that Geotail was behind the quasi-parallel shock from 1920 to 2045 UT.

[14] The subject of a deeper analysis is the time interval from 2015 to 2045 UT that is distinguished by the shadowed area in Figure 2. Figure 3 presents observations of the THEMIS spacecraft ordered according to the distance of a particular spacecraft from the Earth. The first two images show ion energy spectra and magnetic field vector as measured by the outermost THB [*Auster et al.*, 2008; *McFadden et al.*, 2008]. One can note three magnetopause and two bow shock crossings. The last THB magnetopause crossing is followed by the crossings observed by THC, THD, and THE; they are indicated by the vertical lines in the next three images. The last two images present ion energy spectra and magnetic field from THA, and one can identify four magnetopause crossings there.

[15] We would like to stress some features in the ion energy spectrogram of THB. At ≈2036 UT, there is a dropout of energetic particles (first image in Figure 3) suggesting that the upstream bow shock changed from quasi-parallel to quasi-perpendicular. This change is complemented by the increase of the magnetosheath density and temperature.

[16] Analyzing multipoint observations of the magnetopause crossings, their sequence yields the magnetopause speed of ≈44.9 km/s along the normal (−0.936; +0.138; +0.324). These parameters were determined by the timing method [*Russell et al.*, 1983] that uses locations and times of crossings observed by THB-THE (events 3, 4, 5, and 6 in Table 1). We would like to point out that this fast and large (more than 1.6 R_E) magnetopause displacement was connected with significant distortion of the magnetopause surface. The normal to the *Shue et al.* [1998] model surface at the point of the THB magnetopause crossing is (+0.988; −0.093; −0.123), whereas we found an enlarged Z component of the normal in all magnetopause crossings (events 3–6). The other indication of this deformation is the direction of the magnetic field just inbound the magnetopause. In accord with the THEMIS location and a large positive tilt angle (+25°), one would expect that B_Z would be a principal component. Indeed, all THEMIS spacecraft observed the B_Z dominated magnetic field prior to 2020 UT, but the B_X component gradually increases afterward and becomes comparable with B_Z at the magnetopause crossings. Observations of THA reveal that the rotation back to the B_Z dominated orientation occurred between the second and third THA magnetopause crossings. Another check of a presence of the magnetopause deformation provides a comparison of the model magnetic field with observations. The *Tsyganenko and Stern* [1996] model predicts $\vec{B} = (7;3;42)$ nT just prior to the last THB magnetopause crossing, whereas THB observes $\vec{B} = (25;0;30)$ nT. A large B_X component suggests a deformation of the magnetopause surface in the XZ plane, but the fact that B_Y is comparable in both the model and observations does not imply that the magnetopause conserved its shape in the XY plane.

3. Discussion

[17] Since an interpretation of observations is rather difficult, we divide this section into two parts. It is generally expected that the magnetopause and bow shock locations are determined by upstream state, thus the first part deals with the upstream observations, whereas the discussion of the magnetosheath thickness is a subject of the second part.

3.1. Upstream Observations

[18] Upstream observations do not reveal any cause for the observed magnetopause displacement because the solar

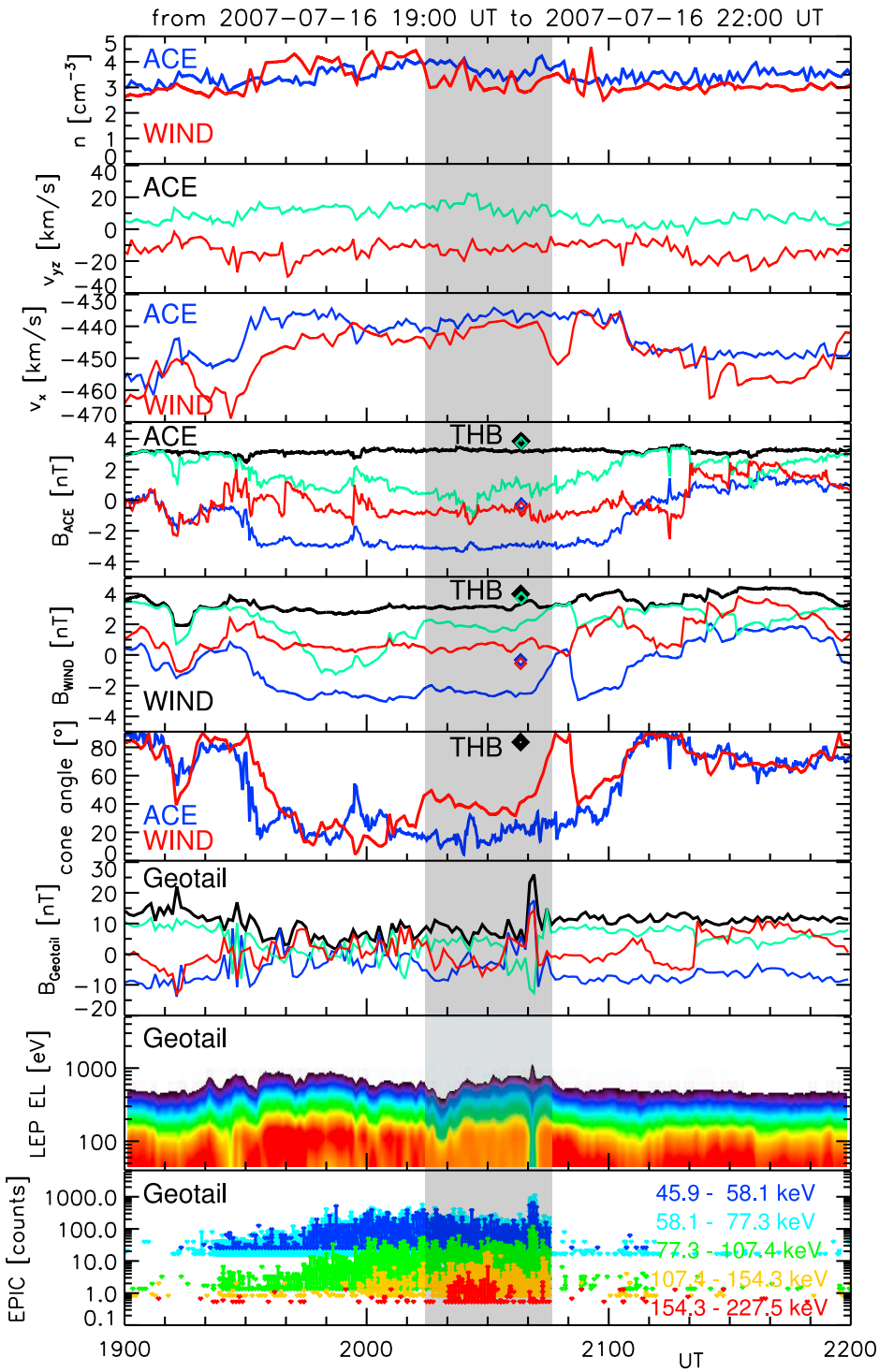

Figure 2. Solar wind data from ACE and Wind, and Geotail magnetosheath observations on July 16, 2007 from 1900 to 2200 UT. From top to bottom: ACE and Wind densities; ACE v_Y (green) and v_Z (red) velocity components; details of ACE and Wind v_X components; three components and strength of ACE IMF; the same data from Wind; cone angles computed from ACE and Wind; three components and strength of the Geotail magnetic field; and Geotail electrons and energetic particles measured by LEP and EPIC. In the magnetic field images, the X component is marked by blue, Y component by green, and Z component by red colors, respectively. The values obtained from THB in the solar wind are indicated by diamonds. The shadowed area indicates the time interval that will be discussed further. Time resolutions of a particular spacecraft were: Wind - 3-s magnetic field and 1-minute plasma data; ACE - 20-s magnetic field and 1-minute plasma data; Geotail - 1-minute magnetic field and plasma data; and THEMIS - 3-s magnetic field and plasma data.

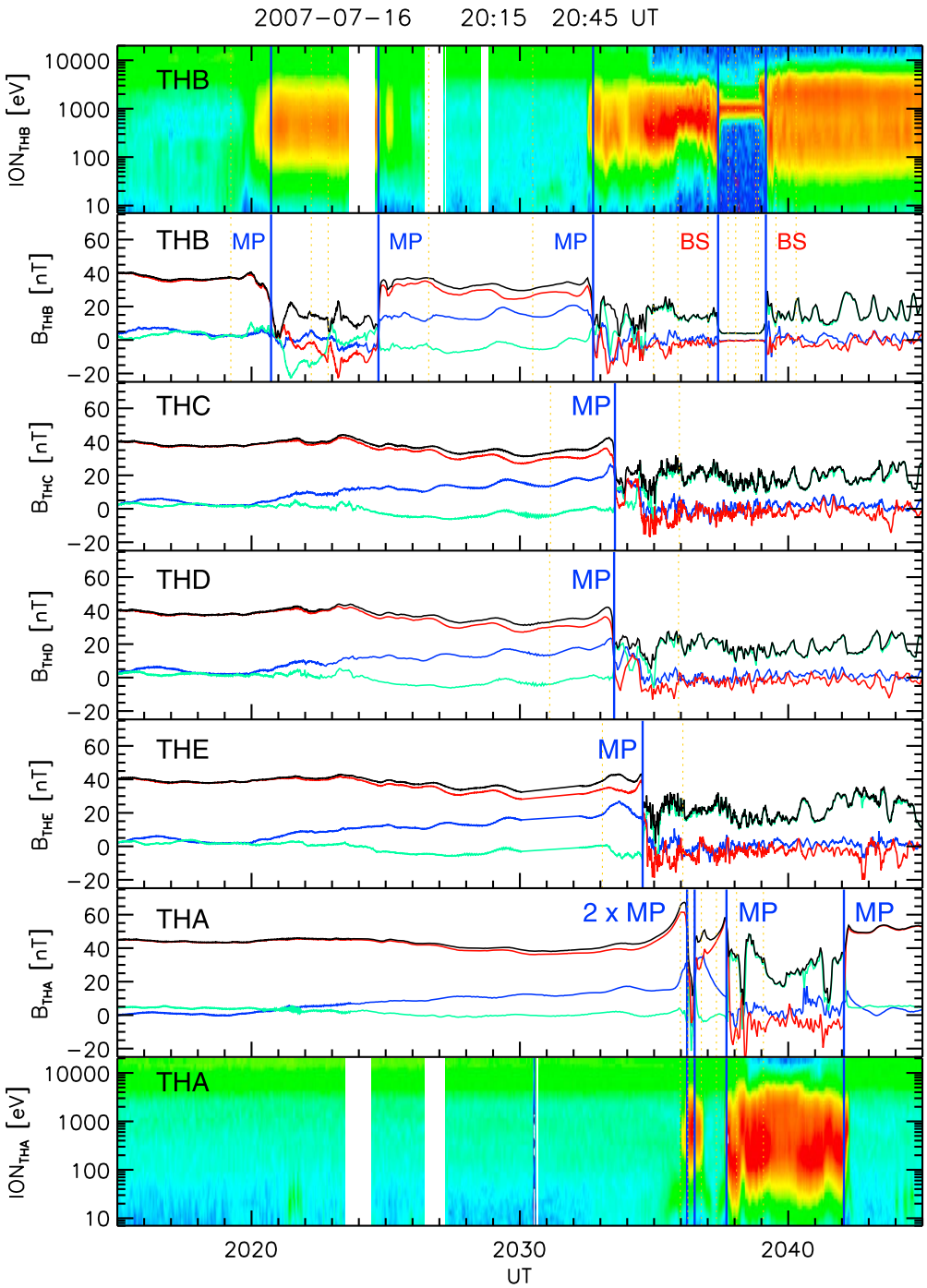

Figure 3. Measurements of THEMIS probes through the interval from 2015 to 2045 UT. From top to bottom: ion spectra from THB, five images of magnetic field observations ordered by the distance of probes from the Earth (THB, THC, THD, THE, THA), and ion spectra from THA. The vertical lines indicate the magnetopause and bow shock crossings. In magnetic field images, B_X, B_Y, B_Z components are marked by blue, green, and red colors, respectively.

wind density and velocity are nearly stable, and the same is true for the IMF magnitude and B_Z component. Small variations of these parameters result in changes of the ram pressure between 1 and 1.4 nPa but the magnetopause beyond THB and/or Geotail locations requires the pressure as low as 0.3 nT (computed according to the *Shue et al.* [1998] model), whereas the magnetopause downstream of THA requires the pressure in excess of 1.5 nPa. However, the B_X and B_Y components change their proportions in the discussed subinterval. We can use three monitors, but their measurements substantially differ. Whereas the ACE cone angle is nearly constant and below 30° during the whole subinterval, Wind shows its sharp increase from ≈30° to ≈50° at 2013 UT and a following new increase to ≈90° at

2045 UT. The best solar wind monitor would be THB that observed the ≈90° cone angle at 2039 UT, but it was in the solar wind only for ≈2 minutes.

[19] We have applied the minimum variance analysis method on observed IMF rotations and found that all of them can be classified as tangential discontinuities (nearly zero normal magnetic field component, negligible changes of the magnetic field magnitude, and plasma parameters across the discontinuity) and that the normals are highly declined (50°–80°) from the solar wind direction. Such discontinuities are hard to propagate.

[20] It has been shown that the IMF fluctuations may be oriented in approximately planar structures that are tilted with respect to the solar wind direction and this causes the IMF propagating from a point of measurement to arrive at other locations with a timing that may be significantly different from what would be expected [*Horbury et al.*, 2001a, 2001b; *Weimer et al.*, 2003; *Weimer and King*, 2008]. One can rely on the typical IMF orientation that is aligned along the Parker spiral, around 45° to the solar wind flow direction, but more sophisticated methods estimate the normal from multispacecraft timing or from gradient methods [e.g., *Russell et al.*, 1983, 2000; *Haaland et al.*, 2004], or use the local field or plasma measurements from a single spacecraft [e.g., *Sonnerup et al.* 2006], or apply different variants of the minimum variance analysis technique [e.g., *Sonnerup and Cahill*, 1967; *Sonnerup and Scheible*, 1998; *Mailyan et al.*, 2008; *Pulkkinen and Rastatter*, 2009]. These propagation methods find minimum variance planes (approximately) perpendicular to the mean magnetic field direction; however, they are based on an assumption of planarity of discontinuity. In our case, this assumption is broken because the discontinuities observed, for example, by Wind would be earlier or later observed by ACE that is not the case. It means that a part of upstream structures is smaller than the ACE-Wind separation or/and that they significantly evolve between the L1 and Earth. We assume that the Earth was affected by a turbulent stream that is missing the ACE location.

[21] For this reason, we are forced to use magnetosheath measurements for an estimation of the IMF direction in front of the bow shock. All monitors register the IMF strength of ≈4 nT. The Geotail magnetic field is about 12 nT until 1920 UT and after 2045 UT, while it is about 5 nT in between. The low compression factor is consistent with the quasi-parallel bow shock in front of Geotail. This conclusion is supported with the presence of energetic particles observed by Geotail (Figure 2, last image) and with the low cone angle measured by ACE. The abrupt decrease of the flux of energetic particles occurred at Geotail at 2045 UT. Moreover, the same effect was observed by THB at ≈2035 UT (first image in Figure 3). We suggest that these changes are caused by an IMF discontinuity arriving at 2035 UT to THB, slowly skimming the bow shock and reaching Geotail approximately 10 minutes later. This discontinuity is denoted as $D1$ hereafter.

[22] As an example of such discontinuity, that observed by Wind at ≈2012 UT can serve (discontinuity $D2$ hereafter). The normal of this discontinuity is (−0.356; −0.933; −0.057) and such discontinuity would skim the bow shock surface with a speed of ≈160 km/s that corresponds to the travel time from Geotail to THEMIS of about 10 minutes. We can point out that similar discontinuities often create HFAs [e.g., *Sibeck et al.*, 1999]; however, in our case, the motional electric field points away from the discontinuity. We should note that the discontinuity $D2$ cannot be a proper cause of the changes observed by THEMIS and Geotail because such discontinuity would propagate from Geotail to THEMIS. We have taken this discontinuity only as evidence that such discontinuities are observed in the solar wind.

[23] Consequently, we cannot rely on the upstream observations, and we should limit ourselves to the indirect evidences that are: (1) The quasi-parallel bow shock in front of THEMIS until 2035 UT; (2) The quasi-parallel bow shock in front of Geotail until 2045 UT; and (3) The B_Y dominated IMF just outbound the subsolar bow shock at ≈2038 UT.

[24] As noted above, these observational facts are consistent with an oblique IMF discontinuity already identified as $D1$. Its normal derived from timing of THB (2035 UT) and Geotail (2045 UT) observations and solar wind speed is about (0.35; −0.93; 0). It should convert a nearly radial IMF that corresponds to the quasi-parallel dayside bow shock to the B_Y dominated IMF observed by THB. Note that this discontinuity is shown by the green dashed-dotted line in Figure 5, and it is discussed in the next section.

[25] The slow motion of the discontinuity along the bow shock leads to situation when the IMF orientation in front of Geotail differs from that at THB for about 10 minutes. This can explain the fact that IMF observed by THB at 2038 UT would lead to the quasi-perpendicular bow shock at Geotail, but it is behind the quasi-parallel one until 2045 UT.

3.2. Magnetosheath Thickness

[26] A geometry of the bow shock (THB) and magnetopause (THA) crossings shown in Figure 3 is illustrated in two images of Figure 4. The red and blue dotted curves stand for the model bow shock [*Formisano et al.*, 1973] and magnetopause [*Shue et al.*, 1998], respectively. Since the spacecraft motion during the analyzed intervals is negligible, only locations at 2036 UT are shown. The straight blue lines depict the estimated magnetopause fronts, while the full red line presents the estimated bow shock front (the numbers correspond to Table 1). Until 2020 UT, the magnetopause is upstream of THB, far away of its model location.

[27] It should be noted that the THEMIS observations on the same day until 2030 UT were analyzed by *Suvorova et al.* [2010] and the authors argued that this effect is caused by a nearly radial IMF orientation (see also [*Merka et al.*, 2003]).

[28] Our attempt to find this effect in the set of ≈6000 magnetopause crossings failed, in spite of its amplitude that follows from the mentioned study. We think that the dependence of the magnetopause position on the IMF cone angle is strongly nonlinear and can be observed only for very small cone angles.

[29] In our case, the small cone angle lasts until ≈2020 UT when the discontinuity arrived to THEMIS and led to the cone angle rise. The discontinuity plane is shown by a green dashed-dotted line in Figure 5. This discontinuity evoked a magnetopause inward motion that resulted in the first magnetopause crossing of THB. Note that the discontinuity is connected with the increase of IMF B_Y and a similar change is seen in the THB magnetosheath observation after the crossing. A new IMF orientation gradually pushes the deformed

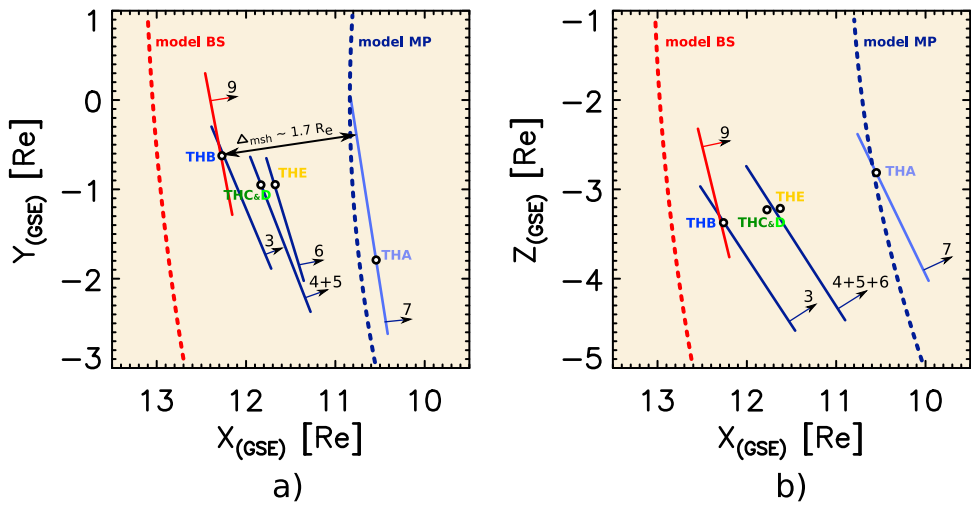

Figure 4. Projections of the THEMIS trajectories onto (a) the *X-Y* and (b) *X-Z* planes (in the GSE system). Model magnetopause [*Shue et al.*, 1998] and bow shock [*Jeřáb et al.*, 2005] are shown by the blue and red dotted curves, respectively. The straight lines show the estimated orientation of the bow shock (red) and magnetopause (blue and black) surfaces. The black arrows display the directions of normals, and the numbers correspond to the events in Table 1.

magnetopause inward and the bow shock follows it and crosses the THB location.

[30] Figure 4a reveals that the magnetosheath is very thin; the projection of the THA–THB separation vector onto the magnetopause normal (we used an average normal of crossings denoted by asterisks in Table 1) yields the value of $\Delta_{msh} = 1.7\ R_E$ that is equal to the thickness determined from the timing of crossings, whereas equation (3) provides a value of 2.3 R_E. Using the magnetopause curvature radius from the *Shue et al.* [1998] model ($a_{mp} = R_C = 10.9\ R_E$) and assuming $\gamma = 5/3$, $M_A = 11$, then equation (4) leads again to the magnetosheath thickness of 2.3 R_E. To receive the observed thickness, the magnetopause curvature radius would be as small as $R_C = 7.8\ R_E$ according to equation (4). The projection onto the XZ plane (Figure 4b) reveals a significant magnetopause deformation that was discussed in the previous section.

[31] We argue that the bow shock and magnetopause normals were determined very reliably because we have received the same results for various time intervals used for their computation. Moreover, the MP normals estimated from the data of the different spacecraft are very similar (Figure 4, Table 1). The bow shock and magnetopause planes (the red and blue lines in Figure 4b) determined at THB and THA locations, respectively, clearly tend to converge to a very small separation at $Z = 0$. Since these two crossings occurred nearly simultaneously, it means that the subsolar magnetosheath is even thinner than we determined from the THB–THA observations.

[32] A possible explanation of the low magnetosheath thickness through its dependence on the IMF cone angle [*Cairns and Lyon*, 1996] can be ruled out for two reasons: (1) This dependence is notable for $M_A \leq 6$ [*Cairns and Grabbe*, 1994], however, $M_A \approx 11$ in our case; and (2) The magnetosheath thinning appears for the cone angles below 20° [*Cairns and Lyon*, 1996] but THB observed the cone angle ≈90° just outbound of the bow shock.

[33] We suggest that the thin magnetosheath is a consequence of a local decrease of the curvature radius results from the magnetopause deformation. The inward magnetopause motion discussed above was observed at the subsolar region, whereas simultaneous outward displacement of the dusk dayside magnetopause was recorded by Geotail. Figure 5 depicts a possible shape of boundaries at ≈2040 UT consistent with the observed crossings. The magnetopause is at (or even downstream of) the THA location and at (or

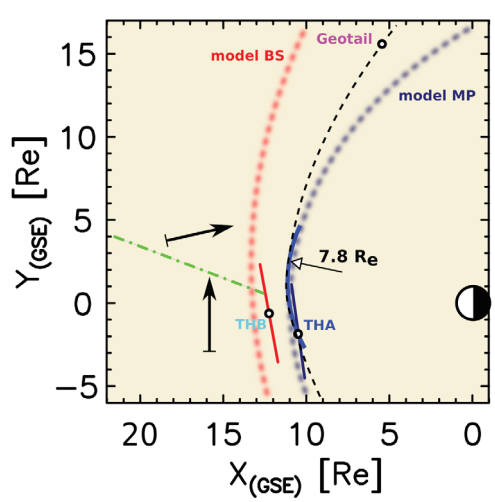

Figure 5. Projections of the observed situation onto the *X-Y* plane. The red and blue dotted curves show the model bow shock and magnetopause, respectively. The thin dashed curve presents estimated magnetopause shape at ≈2042 UT. The green dashed–dotted line stands for the IMF discontinuity estimated from THEMIS and Geotail observations, and IMF orientations shown by the black arrows correspond to those observed by ACE prior to (2015 UT) and by THB after (2038 UT) the discontinuity arrival.

upstream of) the Geotail location. We assume that this very distorted magnetopause shape is caused by the IMF discontinuity discussed above. This discontinuity shown in Figure 5 as the green dashed–dotted line causes the different IMF orientations (black arrows) upstream of THA and Geotail. The exact orientation and position of the discontinuity is unknown, but we know the IMF orientation (purely duskward) at the THB location. However, Geotail was behind the quasi-parallel shock until 2045 UT and it implies a small cone angle. The low cone angle displaces the magnetopause outward at the Geotail position [*Suvorova et al.*, 2010], whereas the large cone angle at THB results in the magnetopause return to a nominal position. This temporal decrease proceeds along the bow shock and leads to a local decrease of the magnetopause curvature radius and thus to corresponding magnetosheath thinning. We would like to stress that the IMF orientation was probably the main factor driving the observed displacements of the boundaries and that this orientation is not necessarily identical along the bow shock surface.

[34] Finally, we can propose the most probable scenario of the event as follows:

[35] 1. The subsolar magnetopause was expanded until 2020 UT due to a radial IMF that causes the decreased magnetosheath pressure [*Suvorova et al.*, 2010].

[36] 2. A tangential discontinuity shaped like that shown in Figure 5 approaches the dawn bow shock flank at 2020 UT and brings the duskward pointing IMF to the parts of the bow shock dawnward of the discontinuity.

[37] 3. The magnetosheath pressure behind the discontinuity increases and pushes the affected parts of the magnetopause inward. This process is responsible for the decreasing curvature radius of the subsolar magnetopause inferred from THEMIS and Geotail observations.

[38] 4. The discontinuity proceeds along the bow shock surface duskward and approaches THB at 2032 UT. Its arrival causes a fast inward motion of both the magnetopause and bow shock.

[39] 5. At 2045 UT, the discontinuity crosses the Geotail location, the expanded magnetopause moves inward and the bow shock becomes quasiperpendicular at this point.

4. Conclusions

[40] We have analyzed a case of simultaneous observations of the dayside magnetopause and bow shock by THEMIS and Geotail. The analysis is supported by ACE and Wind upstream observations propagated to the bow shock. We can conclude that:

[41] (1) Although the precise orientation of the IMF just upstream from Earth's bow shock may differ from that seen far upstream, we showed that oblique IMF discontinuities with large normals transverse to the Sun-Earth line were present in both locations.

[42] (2) Oblique IMF discontinuities result in prolonged intervals of differing IMF orientation upstream from the pre- and post-noon bow shock.

[43] (3) Although not included in any of empirical models, our study suggests that the IMF orientation controls the magnetopause and bow shock positions. However, the effect can be limited to a relatively narrow range of the cone and/or clock angles.

[44] (4) The position of a particular point on the magnetopause is governed by the pressure balance across the magnetopause at this point. At any given time, inward and outward motions at different points of the magnetopause can take place simultaneously according to the difference of corresponding IMF orientations.

[45] (5) IMF directional variations result in large transient deformations of the magnetopause shape.

[46] (6) The deformation of the magnetopause surface exhibiting suppressed curvature radius leads to a transient magnetosheath thinning (to about 70% of its standard value in the reported case).

[47] These conclusions are based on a favorable configuration of the spacecraft and we think that the probability to find a similarly documented case is very low. However, a statistical processing of the data collected by THEMIS, Geotail, and Cluster at the dayside magnetopause can answer the question how frequent are observed phenomena.

[48] **Acknowledgments.** We acknowledge the Geotail team for the magnetic field and plasma data and NASA contract NAS5-02099 and V. Angelopoulos for use of data from the THEMIS mission. Specifically, C. W. Carlson and J. P. McFadden for use of ESA data and K. H. Glassmeier, U. Auster and W. Baumjohann for the use of FGM data provided under the lead of the Technical University of Braunschweig and with financial support through the German Ministry for Economy and Technology and the German Center for Aviation and Space (DLR) under contract 50 OC 0302. The present work was partly supported by the Czech Grant Agency under Contracts 205/09/0170 and 205/09/0112, and partly by the Research Plan MSM 0021620860 that is financed by the Ministry of Education of the Czech Republic. The work at NCU was supported by the grant NSC 98-2811-M-008-043. K. Jelínek thanks the Charles University Grant Agency (GAUK 102508) for support.

[49] Masaki Fujimoto thanks Ken Tsubouchi and another reviewer for their assistance in evaluating this paper.

References

Auster, H. U., et al. (2008), The THEMIS Fluxgate Magnetometer, *Space Sci. Rev.*, *141*, 235, doi:10.1007/s11214-008-9365-9.

Boardsen, S. A., T. E. Eastman, T. Sotirelis, and J. L. Green (2000), An empirical model of the high-latitude magnetopause, *J. Geophys. Res.*, *105*(A10), 23,193–23,219, doi:10.1029/1998JA000143.

Cairns, I. H., and C. L. Grabbe (1994), Towards an MHD theory for the standoff distance of Earth's bow shock, *Geophys. Res. Lett.*, *21*(25), 2781–2784.

Cairns, I. H., and J. G. Lyon (1996), Magnetic field orientation effects on the standoff distance of Earth's bow shock, *Geophys. Res. Lett.*, *23*(21), 2883–2886.

Fairfield, D. H. (1971), Average and unusual locations of the Earth's magnetopause and bow shock, *J. Geophys. Res.*, *76*(28), 6700–6716, doi:10.1029/JA076i028p06700.

Farris, M. H., and C. T. Russell (1994), Determining the standoff distance of the bow shock: Mach number dependence and use of models, *J. Geophys. Res.*, *99*(A9), 17,681–17,689.

Farrugia, C. J., et al. (2008), Two-stage oscillatory response of the magnetopause to a tangential discontinuity/vortex sheet followed by northward IMF: Cluster observations, *J. Geophys. Res.*, *113*, A03208, doi:10.1029/2007JA012800.

Formisano, V., P. C. Hedgecock, G. Moreno, F. Palmiotto, and J. K. Chao (1973), Solar Wind Interaction with the Earth's Magnetic Field, 2. Magnetohydrodynamic Bow Shock, *J. Geophys. Res.*, *78*(19), 3731–3744.

Haaland, S. E., et al. (2004), Four-spacecraft determination of magnetopause orientation, motion and thickness: comparison with results from single-spacecraft methods, *Ann. Geophys.*, *22*, 4, 1347–1365.

Horbury, T. S., D. Burgess, M. Fränz, and C. J. Owen (2001a), Prediction of Earth arrival times of interplanetary southward magnetic field turnings, *J. Geophys. Res.*, *106*, 30,001–30,009.

Horbury, T. S., D. Burgess, M. Fränz, and C. J. Owen (2001b), Three spacecraft observations of solar wind discontinuities, *Geophys. Res. Lett.*, *28*, 677–680, doi:10.1029/2000GL000121.

Jacobsen, K. S., et al. (2009), Themis observations of extreme magnetopause motion caused by a hot flow anomaly, *J. Geophys. Res.*, *114*, A08210, doi:10.1029/2008JA013873.

Jeřáb, M., Z. Němeček, J. Šafránková, K. Jelínek, and J. Merka (2005), A study of bow shock locations, *Planet. Space Sci.*, *53*, 85–94.

Laakso, H., et al. (1998), Oscillations of magnetospheric boundaries driven by IMF rotations, *Geophys. Res. Lett.*, *25*(15), 3007–3010, doi:10.1029/98GL50916.

Lepidi, S., U. Villante, A. J. Lazarus, A. Szabo, and K. Paularena (1996), Observations of bow shock motion during times of variable solar wind conditions, *J. Geophys. Res.*, *101*, 11,107–11,123.

Mailyan, B., C. Munteanu, and S. Haaland (2008), What is the best method to calculate the solar wind propagation delay?, *Ann. Geophys.*, *26*, 2383–2394.

McFadden, J. P., C. W. Carlson, D. Larson, M. Ludlam, R. Abiad, B. Elliott, P. Turin, M. Marckwordt, and V. Angelopoulos (2008), The THEMIS ESA plasma instrument and in-flight calibration, *Space Sci. Rev.*, *141*, 277, doi:10.1007/s11214-008-9440-2.

Merka, J., A. Szabo, J. Šafránková, and Z. Němeček (2003), Earth's bow shock and magnetopause in the case of a field-aligned upstream flow: Observation and model comparison, *J. Geophys. Res.*, *108*(A7), 1269, doi:10.1029/2002JA009697.

Merka, J., A. Szabo, J. A. Slavin, and M. Peredo (2005), Three-dimensional position and shape of the bow shock and their variation with upstream Mach numbers and interplanetary magnetic field orientation, *J. Geophys. Res.*, *110*, A04202, doi:10.1029/2004JA010944.

Němeček, Z., and J. Šafránková (1991), The Earth's bow shock and magnetopause position as a result of the solar wind-magnetosphere interaction, *J. Atmos. Terr. Phys.*, *53*, 1049–1054.

Petrinec, S. M., and C. T. Russell (1996), Near-Earth magnetopause shape and size as determined from the magnetopause flaring angle, *J. Geophys. Res.*, *101*(A1), 137–152, doi:10.1029/95JA02834.

Pudovkin, M. I., M. F. Heyn, and V. V. Lebedeva (1982), Magnetosheath's parameters and their dependence on intensity and direction of the solar wind magnetic field, *J. Geophys. Res.*, *87*(A10), 8131–8138, doi:10.1029/JA087iA10p08131.

Pulkkinen, A., and L. Rastätter (2009), Minimum variance analysis-based propagation of the solar wind observations: Application to real-time global magnetohydrodynamic simulations, *Space Weather*, *7*, S12001, doi:10.1029/2009SW000468.

Russell, C. T., M. M. Mellott, E. J. Smith, and J. H. King (1983), Multiple spacecraft observations of interplanetary shocks: Four spacecraft determination of shock normals, *J. Geophys. Res.*, *88*, 4739–4748.

Roelof, E. C., and D. G. Sibeck (1993), Magnetopause shape as a bivariate function of interplanetary magnetic field Bz and solar wind dynamic pressure, *J. Geophys. Res.*, *98*(A12), 21,421–21,450, doi:10.1029/93JA02362.

Russell, C. T., et al. (2000), The interplanetary shock of September 24, 1998: Arrival at Earth, *J. Geophys. Res.*, *105*, 25,143–25,154.

Šafránková, J., K. Jelínek, and Z. Němeček (2003), The bow shock velocity from two-point measurements in frame of the INTERBALL project, *Adv. Space Res.*, *31*, 5, 1377–1382, doi:10.1016/S0273-1177(02)00951-1.

Seiff, A., and E. E. Whiting (1962), Correlation study of bow-wave profiles on blunt bodies, 62N10002, Report Number: NASA-TN-D-1148.

Shue, J.-H., J. K. Chao, H. C. Fu, K. K. Khurana, C. T. Russell, H. J. Singer, and P. Song (1997), A new functional form to study the solar wind control of the magnetopause size and shape, *J. Geophys. Res.*, *102*(A5), 9497–9511, doi:10.1029/97JA00196.

Shue, J.-H., et al. (1998), Magnetopause location under extreme solar wind conditions, *J. Geophys. Res.*, *103*(A8), 17,691–17,700.

Sibeck, D. G., R. E. Lopez, and E. C. Roelof (1991), Solar wind control of the magnetopause shape, location, and motion, *J. Geophys. Res.*, *96*(A4), 5489–5495, doi:10.1029/90JA02464.

Sibeck, D. G., et al. (1999), Comprehensive study of the magnetospheric response to a hot flow anomaly, *J. Geophys. Res.*, *104*(A3), 4577–4593, doi:10.1029/1998JA900021.

Sibeck, D. G., et al. (2000), Magnetopause motion driven by interplanetary magnetic field variations, *J. Geophys. Res.*, *105*, A11, 25155–25169, doi:10.1029/2000JA900109.

Sonnerup, B. U. Ö., and L. J. Cahill Jr. (1967), Magnetopause structure and altitude from Explorer-12 observations, *J. Geophys. Res.*, *72*, 171–183.

Sonnerup, B. U. Ö., and M. Scheible (1998), Minimum and maximum variance analysis, in *Analysis Methods for Multi-spacecraft Data*, edited by G. Paschmann and P. W. Daly, ISSI SR-001, pp. 185–220, ESA Publ. Div., Noordwijk, Netherlands.

Sonnerup, B. U. Ö., S. Haaland, G. Paschmann, M. W. Dunlop, H. Rème, and A. Balogh (2006), Orientation and motion of a plasma discontinuity from single-spacecraft measurements: Generic residue analysis of Cluster data, *J. Geophys. Res.*, *111*, A05203, doi:10.1029/2005JA011538.

Spreiter, J. R., A. L. Summers, and A. Y. Alksne (1966), Hydromagnetic flow around the magnetosphere, *Planet. Space Sci.*, *14*, 223–253.

Suvorova, A. V., J.-H. Shue, A. V. Dmitriev, D. G. Sibeck, J. P. McFadden, H. Hasegawa, K. Ackerson, K. Jelínek, J. Šafránková, and Z. Němeček (2010), Magnetopause expansions for quasi-radial interplanetary magnetic field: THEMIS and Geotail observations, *J. Geophys. Res.*, doi:10.1029/2010JA015404, in press.

Tsubouchi, K., T. Terasawa, T. Mukai, Y. Saito, T. Yamamoto, S. Kokubun, H. Kojima, and H. Matsumoto (2000), Motion of the Earth's bow shock in the deep-tail flank, *J. Geophys. Res.*, *105*(A11), 25,097–25,112, doi:10.1029/1999JA000454.

Tsyganenko, N. A., and D. P. Stern (1996), A new-generation global magnetosphere field model based on spacecraft magnetometer data, *ISTP Newsl. 6/1* 21.

Weimer, D. R., and J. H. King (2008), Improved calculations of interplanetary magnetic field phase front angles and propagation time delays, *J. Geophys. Res.*, *113*, A01105, doi:10.1029/2007JA012452.

Weimer, D. R., D. M. Ober, N. C. Maynard, M. R. Collier, D. J. McComas, N. F. Ness, C. W. Smith, and J. Watermann (2003), Predicting interplanetary magnetic field (IMF) propagation delay times using the minimum variance technique, *J. Geophys. Res.*, *108*(A1), 1026, doi:10.1029/2002JA009405. (Correction, *J. Geophys. Res.*, *109*, A12104, doi:10.1029/2004JA010691, 2004.)

Zhang, H., Q. G. Zong, D. G. Sibeck, T. A. Fritz, J. P. McFadden, K.-H. Glassmeier, and D. Larson (2009), Dynamic motion of the bow shock and the magnetopause observed by THEMIS spacecraft, *J. Geophys. Res.*, *114*, A00C12, doi:10.1029/2008JA013488.

K. Jelínek, Z. Němeček, and J. Šafránková, Faculty of Mathematics and Physics, Charles University, V Holešovičkách 2, 180 00 Prague 8, Czech Republic.

J.-H. Shue and A. V. Suvorova, Institute of Space Science, National Central University, Jhongli, Taiwan.

D. G. Sibeck, NASA Goddard Flight Center, Greenbelt, MD 20771, USA.